



# Photocatalytic degradation of metoprolol by TiO<sub>2</sub> nanotube arrays and UV-LED: Effects of catalyst properties, operational parameters, commonly present water constituents, and photo-induced reactive species

Y. Ye<sup>a,b,\*</sup>, Y. Feng<sup>a</sup>, H. Bruning<sup>a</sup>, D. Yntema<sup>b</sup>, H.H.M. Rijnhaarts<sup>a</sup>

<sup>a</sup> Sub-Department of Environmental Technology, Wageningen University, Bornse Weilanden 9, 6708WG, Wageningen, The Netherlands

<sup>b</sup> Wetsus, European Centre of Excellence for Sustainable Water Technology, Oostergoweg 9, 8911 MA Leeuwarden, The Netherlands



## ARTICLE INFO

**Keywords:**  
TiO<sub>2</sub> nanotubes  
Metoprolol  
Photocatalysis  
UV-LED  
Scavengers

## ABSTRACT

The aim of this study was to evaluate the use of self-organized TiO<sub>2</sub> nanotube arrays (TNAs) as immobilized catalyst and UV-LED as light source (UV-LED/TNAs) for photocatalytic degradation of the  $\beta$ -blocker metoprolol (MTP) from aqueous solution. Firstly we employed electrochemical anodization to synthesize self-organized TNAs, and the effect of anodization potential and annealing temperature was examined. Characterization by SEM demonstrated a linear relation between the diameter of TiO<sub>2</sub> nanotubes produced and the anodization potential, while Raman measurement revealed the vital role of annealing on crystallographic composition of the anodic produced TiO<sub>2</sub> nanotubes. Regarding their performance in photocatalytic MTP degradation, surface morphology and crystallographic composition of the TNAs were found to impose crucial influence: only TNAs with diameter not smaller than 53 nm enabled rapid MTP degradation, and highest MTP degradation was obtained when a mixture of anatase and rutile were present in the TNAs. Secondly, the effect of operational parameters, *i.e.* initial MTP concentration, pH, was investigated. Initial MTP concentration at low level had no detrimental effect on the process performance. Rapid MTP degradation and high total removal were achieved in a wide pH range (3–11). To evaluate the applicability of TNAs for water treatment, experiments were first carried out in the presence of three different commonly present water constituents, *i.e.* bicarbonate ions, phosphate ions, and natural organic matters (NOMs). The results show that bicarbonate and phosphate ions have no inhibitory effect at concentration levels up to 200 mg/L, and NOMs exhibit detrimental effect when their concentration exceeds 5 mg/L. The total removal MTP degradation reduced from  $87.09 \pm 0.09\%$  to  $62.05 \pm 0.08\%$  when tap water samples were applied, demonstrating reasonable efficacy for practical applications. Regarding the degradation mechanism, formic acid and tert-butanol were added as scavenger for photo-generated holes ( $h^+$ ) and hydroxyl radicals ( $\cdot OH$ ), respectively. The obtained results demonstrate that primary degradation process occurred in liquid phase with participation of hydroxyl radicals in the liquid phase ( $\cdot OH_{liquid}$ ), while smaller portion of MTP were degraded on the catalysis surface via reaction with  $h^+$  and hydroxyl radicals adsorbed on the catalyst surface ( $\cdot OH_{surface}$ ). Other reactive species, *e.g.* photo generated electrons and superoxide radical anions, did also play a minor role in MTP degradation. The mechanistic aspect was further confirmed by identification of degradation products by LC-MS/MS. The TNAs exhibited good stability after repeated use under varied operation conditions.

## 1. Introduction

In recent years, a large number of pharmaceuticals have been detected at various concentration levels in the aqueous environment [1,2], from ground and surface water to even drinking water resources [2–9]. This issue is gaining concerns because of the potential risks for aquatic life and human society. On the other hand, the presence of such pollutants in various water bodies together with treatability studies

clearly demonstrate the poor efficacy of conventional wastewater treatment processes and drinking water production processes on removal of wide range of pharmaceutical compounds [3,10,11]. Among the wide range of pharmaceutical compounds frequently detected in the environment, a  $\beta$ -blocker, *i.e.* metoprolol (MTP), is considered to be an emerging contaminant: (1) it has been classified in the group of pharmaceuticals most commonly present in the environment [2]; (2) it is widely used in both hospitals and households, and enters surface waters

\* Corresponding author at: Sub-Department of Environmental Technology, Wageningen University, Bornse Weilanden 9, 6708WG, Wageningen, The Netherlands.  
E-mail addresses: [yeyin01@hotmail.com](mailto:yeyin01@hotmail.com), [yin.ye@wur.nl](mailto:yin.ye@wur.nl) (Y. Ye).

(including drinking water sources) at up to  $\mu\text{g/L}$  level [12]; (3) environmental risk assessment studies have indicated environmental risks associated with its presence [13,14]. Therefore, removal of such compounds from aqueous streams, especially during drinking water production, has become an urgent topic, to guard the safety of water supply and improve the quality of life.

Advanced oxidation processes (AOPs), where a strong oxidizing species hydroxyl radical ( $\cdot\text{OH}$ ) is the primary oxidant, exhibit sufficient efficacy in elimination of a wide range of organic contaminants including pharmaceuticals [15–17], among which photocatalysis is considered to be a good approach because of its chemical-free nature. Although many semiconductors have photocatalytic activity,  $\text{TiO}_2$  is the most used photocatalyst in environmental applications including air pollution control [18] and water treatment [11], because of its low toxicity, low cost, high efficiency, and high stability. Principles of  $\text{TiO}_2$  photocatalytic processes have been described elsewhere [12,19]. The photocatalytic degradation of organic pollutants is usually initiated by excitation of  $\text{TiO}_2$  by photons containing energy higher than the  $\text{TiO}_2$  band gap. Sequentially, electron/hole ( $e^-/\text{h}^+$ ) pairs are generated on the catalyst surface. The photo-generated electrons and holes are able to participate in direct redox reactions with target organic contaminants. Besides, the photo-generated electrons and holes can also react with oxygen, water, or  $\text{HO}^-$  to generate highly reactive species, e.g. hydroxyl radicals ( $\cdot\text{HO}$ ), superoxide radical anions ( $\text{O}_2\cdot^-$ ), etc, and those in-situ generated reactive species are able to oxidize and reduce many contaminants. Applicability of  $\text{TiO}_2$  for elimination of a wide range of organic contaminant has been well documented [20–24].

Recently, regarding real life application, attempts have been made to employ immobilized catalyst for elimination of organic pollutants from aqueous streams [20,25–29], in order to achieve better retention and reuse of the catalyst. Among all kinds of immobilized  $\text{TiO}_2$ , the self-organized  $\text{TiO}_2$  nanotube arrays (TNAs) exhibit great potential because of its relatively large surface area, high stability, and oriented electron transport as well as high electron mobility which could reduce electron/holes ( $e^-/\text{h}^+$ ) recombination in the material [30,31]. Although there are various approaches for  $\text{TiO}_2$  nanotube arrays synthesis, electrochemical anodization has gained the most attention because it is a fast and facile method [32], and easy to tune the morphology of  $\text{TiO}_2$  nanotubes produced. Synthesis of  $\text{TiO}_2$  nanotube arrays via anodization of Ti material has been previously studied by other researchers [30,33–35]. Among various factors exerting impact on the characteristics of anodic produced  $\text{TiO}_2$  nanotube arrays, anodization potential and annealing temperature are two vital parameters which control the diameter and crystallographic structure of the  $\text{TiO}_2$  nanotube arrays, respectively [36,37]. Furthermore, the diameter and crystallographic structure are reported to impose impact on photocatalytic performance of the  $\text{TiO}_2$  nanotube arrays [38,39]. The use of  $\text{TiO}_2$  nanotube arrays for photocatalytic removal of organic pollutants has received attention, and examples are available in literature [32,39–41].

Regarding implications of photocatalysis, light source is another vital factor because it imposes significant impact on the operational and maintenance costs. Mercury lamps have been widely used for photocatalytic pollutants elimination processes, which are reported to have major drawbacks: (1) short working life span (500–2000 h); (2) hazardous materials (mercury) content; (3) fragility [42]. Recent advances in light emitting diode (LED) technology provides better alternative, due to their advantages: short warm-up time, no hazardous materials content, long working life span, compatibility, narrow light emission spectra, etc [42]. Therefore, in recent years the use of UV-LED for photocatalytic treatment of various organic contaminants is gaining research interests [43–45]. Only very few attempts have been made to combine the use of TNAs and UV-LED, for dye degradation [41].

To the best of the authors' knowledge, no research has been conducted on the photocatalytic treatment of pharmaceutical compounds using self-organized TNAs as catalyst and UV-LED as light source. In this context, in the present study we aimed to evaluate the performance

of the combination of self-organized TNAs as immobilized catalyst and UV-LED as light source (UV-LED/TNAs) for photocatalytic degradation of the  $\beta$ -blocker MTP from aqueous solution. Synthesis and characterization of the self-organized  $\text{TiO}_2$  nanotube arrays was studied, and the effect of two operational parameters, i.e. anodization potential and annealing temperature, on the properties of  $\text{TiO}_2$  nanotube arrays was examined. Moreover, the impact of  $\text{TiO}_2$  nanotube arrays' characteristics on their photocatalytic performance was studied. Regarding photocatalytic degradation of MTP over  $\text{TiO}_2$  nanotube arrays, the effect of multiple operational parameters and the effect of back ground water constituents were investigated. Additionally, its applicability in drinking water was investigated by conducting experiments in tap water samples. Furthermore, experiments with addition of specific scavengers were carried out to understand the mechanistic aspect, and contributions of the different reactive species and reaction mechanism were identified. The stability of TNAs in the UV-LED/TNAs photocatalytic system was also evaluated.

## 2. Materials and methods

### 2.1. Chemicals

Titanium foil ( $\geq 99.5\%$ , 0.3 mm thick) was purchased from the Titaniumshop (The Netherlands). Ammonium sulphate ( $\geq 99.0\%$ ), ammonium fluoride ( $\geq 98.0\%$ ), *tert*-Butanol ( $\geq 99.0\%$ ), formic acid ( $\geq 96\%$ ) were obtained from Sigma-Aldrich (Germany). Metoprolol tartrate salt ( $\geq 98.0\%$ ) was purchased from Sigma-Aldrich (Germany) and was used as received. Stock solution of metoprolol tartrate salt was prepared at MTP concentration of 200 mg/L. Acetone ( $\geq 99.7\%$ ), 2-propanol ( $\geq 99.9\%$ ), sodium carbonate ( $\geq 99.9\%$ ), hydrochloric acid (0.1 mol/L), tri-sodium phosphate dodecahydrate ( $\geq 98.0\%$ ), and sodium hydroxide aqueous solution (1 mol/L) were purchased from VWR (Belgium) and was used as received. An aquatic NOM Suwannee River NOM (2R101N) was obtained from International Humic Substances Society (IHSS) and received as dry solid extracts. Stock solution of the Suwannee River NOM was prepared at concentration of 100 mg/L. Ultrapure water from a Milli-Q Advantage A10 system (Merck Millipore, Darmstadt, Germany) was used for preparation of stock solutions and reaction solutions.

### 2.2. Synthesis of $\text{TiO}_2$ nanotube arrays by electrochemical anodization

As pretreatment, the Ti foils were first degreased by successively ultra-sonication for 15 min in 2-propanol, acetone and Milli-Q water, and then were dried in  $\text{N}_2$  atmosphere. The  $\text{TiO}_2$  nanotube arrays (TNAs) were synthesized by electrochemical anodization in a two-electrode chemical cell connected to an EST150 DC power supply (Delta Elektronika, The Netherlands). A Ti foil with a size of 3 cm  $\times$  4.5 cm was used as anode, and a stainless steel foil with a size of 4.5 cm  $\times$  5 cm was used as cathode. The distance between the electrodes was 2 cm. The Ti foil was anodized in 100 mL aqueous electrolyte (0.15 mol/L  $\text{NH}_4\text{F}$  + 1 mol/L  $(\text{NH}_4)_2\text{SO}_4$ ) [46] under designated voltage for 2 h. Then the obtained foil was first rinsed and then further sonication washed with Milli-Q water to remove residue electrolyte and impurities on the surface. Subsequently, the treated Ti foil was annealed at designated temperatures for 0.5 h in a furnace (Nabertherm, Germany) in air atmosphere and was cooled gradually back to ambient temperature after annealing. The designated anodization potentials and corresponding annealing temperatures for synthesis of different TNAs are summarized herein in Table 1.

### 2.3. Characterization of $\text{TiO}_2$ nanotube arrays

The surface morphologies of the prepared TNAs were characterized by scanning electron microscopy (SEM) and the chemical composition of the prepared TNAs was measured by EDX. The SEM/EDX analyses

**Table 1**

Anodization potentials and annealing temperatures for different TNAs samples.

Sample	Anodization potential (V)	Annealing temperature (°C)
1	1	450
2	5	450
3	10	450
4	15	450
5	20	450
6	25	450
7	20	No annealing
8	20	300
9	20	600

were performed using a JEOL JSM 6480 scanning electron microscope (JEOL Europe B.V., Nieuw-Vennep, The Netherlands) equipped with a EDX system. Surface area measurements of TNAs samples prepared under different anodization potentials were performed using a Tristar 3000 Surface area and Porosity Analyzer (Micromeritics, USA), where nitrogen adsorption isotherms were collected at 77 K ( $-196^{\circ}\text{C}$ ) and the Brunauer-Emmett-Teller model was used to determine the specific surface area. Raman spectra of the prepared TNAs samples were recorded using a Horiba LabRAM spectrometer equipped with a mpc3000 laser (532.2 nm), an 800 mm focal length achromatic flat field monochromator (grating of 600 grooves/mm) and a Synapse multichannel air cooled ( $-70^{\circ}\text{C}$ ) CDD detector.

#### 2.4. Photocatalytic degradation of metoprolol

The photocatalytic experiments were conducted in a Petri dish with a 450 mW UV-LED light source module placed on the top. The UV-LED light source module consisted of a UV-LED (NCSU033B, NICHIA, Japan) and has peak emission wavelength of 365 nm, and an aluminum plate served as heat dispenser. A schematic of the set-up is shown in Fig. 1. The experiments were carried out with a reaction solution volume of 60 mL, with presence of desired TNAs (size of 3 cm  $\times$  3 cm), at ambient temperature. The distance between the UV-LED and the surface of TNAs was 2 cm. Continuous mixing started as soon as the reaction solution was added into the Petri dish. Before switching on the UV-LED, the reaction system was kept in dark for 1 h to establish saturation of any possible adsorption of MTP on TNAs surface. Then the photocatalytic experiments started, for duration of 120 min. The radiant power of the UV-LED reached the surface of TNAs was 1.9 mW/cm<sup>2</sup>, measured by a THORLABS S150C radiant power meter (THORLABS, USA). 1 mL samples were taken at designated time intervals, and stored in dark at 4 °C till LC-MS/MS analysis. All experiments were carried out in duplicate. Except for experiments conducted in designated acid or alkaline conditions, all other experiments were conducted

**Table 2**

Characteristics of the tap water.

Parameters	Unit	Values
Cl	mg/l	60.1
NO <sub>2</sub> <sup>-</sup>	mg/l	< 0.05
NO <sub>3</sub> <sup>-</sup>	mg/l	8.84
PO <sub>4</sub> <sup>3-</sup>	mg/l	< 0.05
SO <sub>4</sub> <sup>2-</sup>	mg/l	1.75
TC	mg/l	53.6
NPOC	mg/l	4.26
IC	mg/l	49.3
Ca <sup>2+</sup>	µg/l	38100
Cu <sup>2+</sup>	µg/l	108
K <sup>+</sup>	µg/l	2360
Mg <sup>2+</sup>	µg/l	9360
Na <sup>+</sup>	µg/l	66600

with natural initial pH (circum-neutral: 6–7) and no pH adjustment was applied.

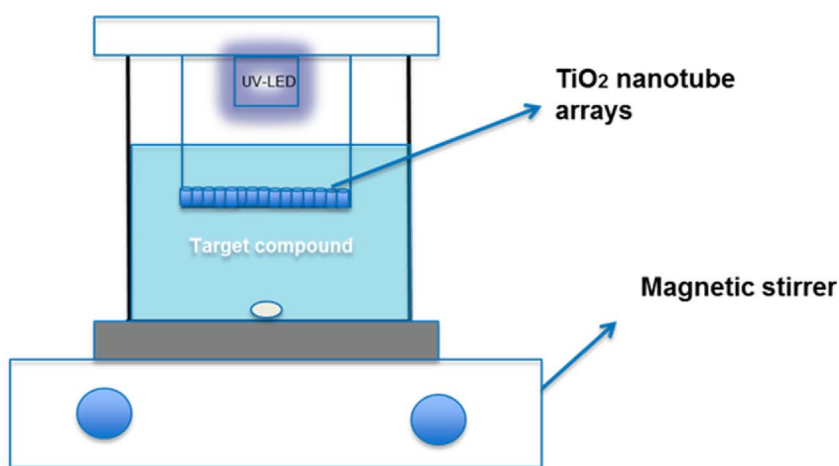
For experiments regarding effect of initial MTP concentration, different initial MTP concentrations ranging from 0.1 mg/L to 1.5 mg/L were applied, while the initial MTP concentration in all other experiments were set to be 1.0 mg/L. For experiments regarding the effect of background water constituents, NOMs, bicarbonate ions, or phosphate ions were added separately to the reaction solutions to designated concentration levels, and pH was adjusted using HCl standard solution to circum-neutral (6–7). For experiments regarding performance in tap water, real tap water (characteristics of the tap water are summarized in Table 2) was used to prepare the reaction solution, while all other experiments were conducted in Milli-Q water. For experiments regarding the effect of initial pH, HCl or NaOH standard solutions were used to adjust the initial pH of the reaction solutions to designated value. For mechanistic study, certain amount of specific scavengers (*tert*-butanol for ·OH, and formic acid for h<sup>+</sup>) were added separately in accordance with a previous study [47].

It should be noticed that MTP does not absorb photons with wavelength longer than 290 nm (Figure SI 2), so no direct photolysis of MTP could take place in our system.

#### 2.5. Analytical procedures

For MTP concentrations and degradation by-products measurement, an Agilent LC-MS/MS system consisting of Agilent infinity 1260 LC-system (degasser, binary pump, auto sampler with cooled tray and column oven) and Agilent 6420 triple Quadrupole Mass Spectrometer with Electrospray ion source was used. More detailed information of the analytical method used can be found in our previous study [48].

Fig. 1. Schematic of the experimental set-up.



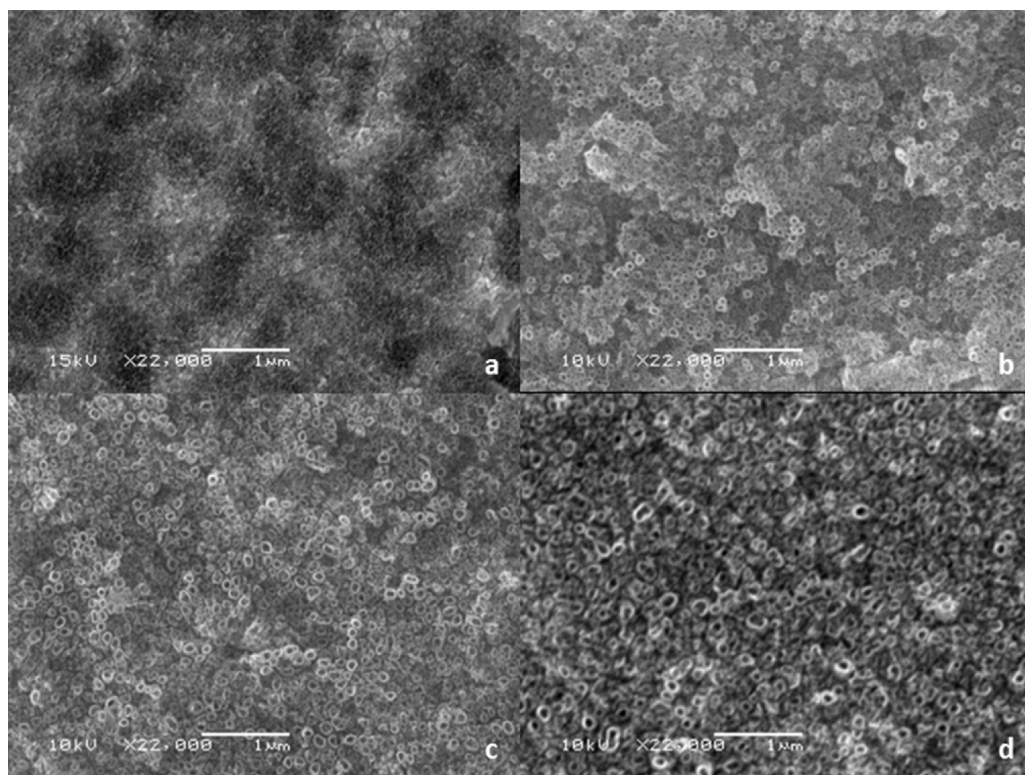


**Fig. 2.** SEM top view images of  $\text{TiO}_2$  nanotube arrays prepared under different anodization potentials: a) anodization potential = 10 V; b) anodization potential = 15 V; c) anodization potential = 20 V; d) anodization potential = 25 V. All samples were annealed at 450 °C for 30 min.

### 3. Results and discussion

#### 3.1. Synthesis of $\text{TiO}_2$ nanotube arrays

Synthesis of  $\text{TiO}_2$  nanotubes (TNT) arrays via anodization of Ti material has been previously studied by other researchers [30,33–35]. Among various factors exerting impact on the characteristics of anodic produced TNAs, anodization potential and annealing temperature are two vital parameters which control the diameter of the TNTs and crystallographic structure of the  $\text{TiO}_2$ , respectively [36,37]. It should be noticed that those impacts may vary among different systems. Therefore, experiments were performed to examine the effect of anodization potential and annealing temperature on the characteristics of  $\text{TiO}_2$  nanotube arrays in our applied system.

##### 3.1.1. Effect of anodization potential

The results (Fig. 2 and Fig. 3) show that anodization potential imposes effects on two aspects of the anodized Ti foil surface. Firstly, a certain threshold anodization potential is needed to achieve total

oxidation of the Ti foil surface to  $\text{TiO}_2$ . As demonstrated in Fig. 3, complete oxidation, revealing the formation of  $\text{TiO}_2$ , was only achieved in samples anodized under potential higher than 10 V, while the atomic percentage of Ti was still rather high in samples anodized under 1 V and 5 V. In addition, a significant amount of F (approx. 2 atomic%) entered the TNTs structures, which is in line with other work using fluoride containing electrolytes [36].

As can be seen in Fig. 2, anodization potential exerts vital impact on diameters of the produce TNAs. Self-organized TNAs structure were formed when applied anodization potential was higher than 10 V, while no tubular nanostructure was obtained on samples anodized under 1 V and 5 V, revealing that threshold anodization potential exists to trigger the growth of TNAs. In those samples with formation of TNAs, anodization potential exerts large effect on the average diameters of formed TNTs, and a clear anodization potential dependence of the TNAs diameter was observed: the average diameter of  $\text{TiO}_2$  nanotubes increased from 26 nm to 106 nm with increased anodization potential from 10 V to 25 V (Fig. 4). This is in accordance with previous studies. Yasuda, K. and P. Schmuki studied the parameters to control morphology and composition of anodic formed self-organized zirconium titanate TNAs,

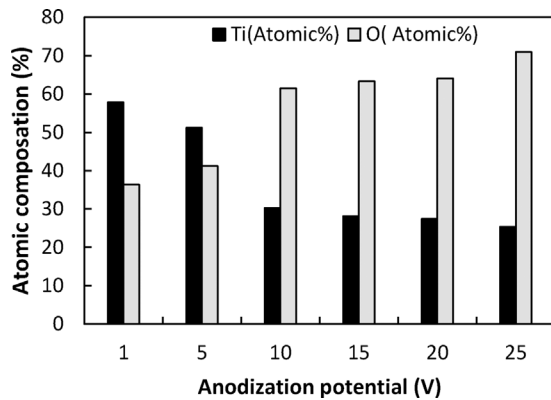


**Fig. 3.** Effect of anodization potential on the atomic composition of anodized Ti foil surface.

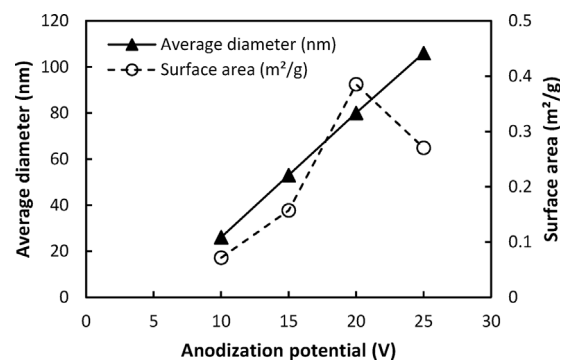


**Fig. 4.** Effect of anodization potential on average  $\text{TiO}_2$  nanotube diameter and  $\text{TiO}_2$  nanotube arrays specific surface area.

and found a linear correlation between the applied anodization potential and the diameter of TNAs in the range between 1 V and 100 V in electrolytes containing ammonium sulphate and ammonium fluoride [49]. Another study conducted by Macak et al. has reported that  $\text{TiO}_2$  nanotubes diameter is linearly dependent by the anodization potential (from 2 V to 40 V) in glycerol/water/ammonium fluoride electrolytes [50]. The slope of the dependencies are different, which could be attributed to the different conductivity of electrolytes used in different studies which imposes large impact on the effective potential on the electrodes [37]. This linear correlation between TNTs diameter and the applied anodization voltage has significant potential for expanding application of TNAs, because based on which tailored TNAs with specific diameters could be produced. Moreover, specific surface area of TNAs was also affected by anodization potential, as shown in Fig. 4. The specific surface area of TNAs increased with increasing anodization potential from 10 V to 20 V, while further increased anodization potential resulted in a decreased specific surface area.

### 3.1.2. Effect of annealing temperature

Many researchers have reported that as-prepared TNAs are typically mainly in an amorphous form [30,36,46], which has low photoactivity. Therefore, annealing is a crucial step to convert the amorphous  $\text{TiO}_2$  into desired crystalline phase to improve photoactivity of the TNAs. To examine this aspect, TNAs were annealed under three different temperatures. The crystallographic structures were characterized using Raman spectroscopy, as described in the previous section regarding measurement methods. The results (Fig. 5) demonstrate that TNAs annealed at 300 °C and 450 °C are present in anatase form, while TNAs annealed at 600 °C have converted to a mixture of rutile and anatase. This is in accordance with previous studies [36]. Interestingly, a peak at around 197  $\text{cm}^{-1}$  was also observed in the as-prepared TNAs, implying the presence of anatase in the as-prepared sample.

## 3.2. Photocatalytic degradation of metoprolol using $\text{TiO}_2$ nanotube arrays as photocatalyst

### 3.2.1. Effect of $\text{TiO}_2$ nanotube arrays characterizations

Although the diameter and crystallographic structure of a TNAs are reported to impose impact on their photocatalytic performance [38,39], the interactions between catalyst and specific target pollutants can be influenced by the structure of the target pollutants [29], and therefore the effect of TNAs properties may differ among different target pollutants. Therefore, the effect of TNAs characterizations on UV-LED/TNAs MTP degradation was investigated experimentally.

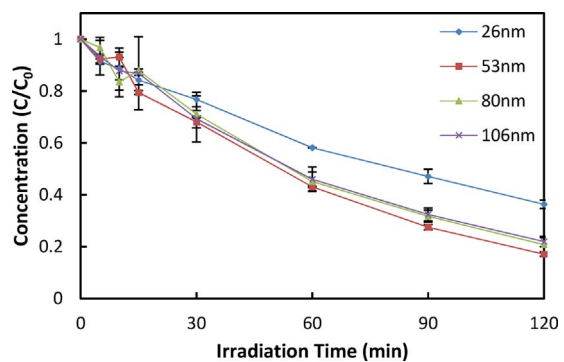
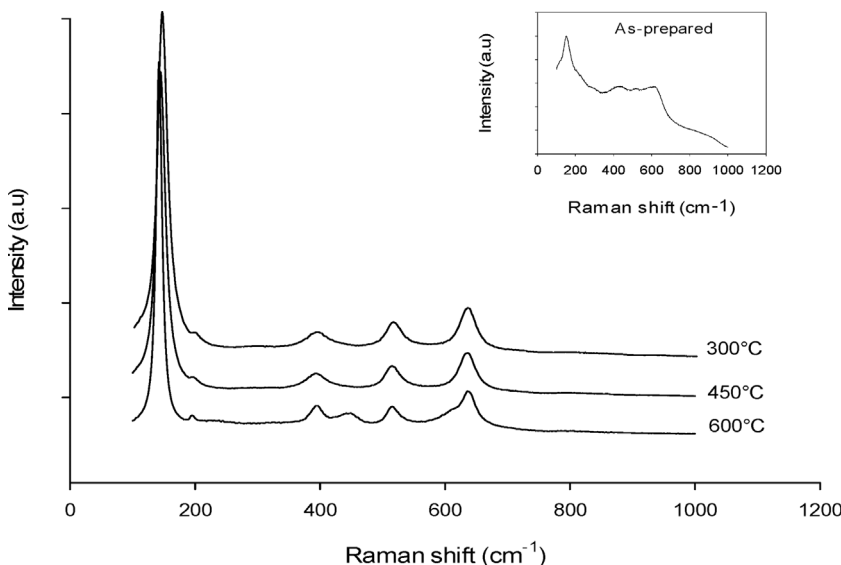


Fig. 6. Effect of  $\text{TiO}_2$  nanotube diameters on the photocatalytic MTP degradation.

**3.2.1.1.  $\text{TiO}_2$  nanotubes surface morphology.** The effect of  $\text{TiO}_2$  nanotube diameters on the efficacy of photocatalytic degradation of MTP was evaluated with 4 TNAs produced under anodization potentials ranging from 10 to 25 V, which corresponds to 4 TNAs arrays with average diameters ranging from 26 to 106 nm. The results (Fig. 6) show that photocatalytic degradations of MTP follow pseudo-first order kinetic model with good correlation ( $R^2 > 0.99$ ). The kinetic data and the total removal of MTP after 120 min photocatalytic degradation under different conditions are summarized and shown in Table 3, it should be noticed that all pseudo-first order rate constant values ( $k_{\text{app}}$ ) in this study were calculated from experimental data of the whole treatment time. From the results shown herein, the 26 nm diameter TNAs have lowest photoactivity: the pseudo-first order rate constant is  $0.0086 \pm 0.0000 \text{ min}^{-1}$ , with a total removal of MTP of  $63.66 \pm 1.65\%$  after 120 min. By increasing the diameter to 53 nm, photoactivity of the TNAs increases significantly: the pseudo-first order rate constant increased by a factor of 67% to  $0.0144 \pm 0.0002 \text{ min}^{-1}$ , and the total removal of MTP increased from  $63.66 \pm 1.65\%$  to almost  $82.88 \pm 0.85\%$ . However, further increasing diameters to 80 nm and 106 nm does not exert significant impact on the MTP degradation. This finding is in accordance with a previous study conducted by Zhuang et al. [38] using TNAs for photocatalytic degradation of Methyl Orange dye. Those authors have reported that TNAs with diameters of 55 nm, 100 nm, and 125 nm have almost the same photoactivity, which was likely resulted from two facts: (1) the specific surface area of the TNAs decreases with increasing tube diameter resulting in a negative impact; (2) the increasing tube diameter on the other hand increases light penetration and absorption inside the tubular structure which affects the photoactivity positively [38]. In the present study, the MTP

Fig. 5. Raman patterns of  $\text{TiO}_2$  nanotube arrays annealed at different temperatures for 30 min. Raman pattern of as-prepared  $\text{TiO}_2$  nanotube arrays without annealing is also given, as an inset. Anodization potential = 20 V.

**Table 3**

Effect of  $\text{TiO}_2$  nanotube diameters on the kinetics of photocatalytic degradation of metoprolol.

Nanotube diameter (nm)	$k_{\text{app}}$ ( $\text{min}^{-1}$ )	$R^2$	Total removal
26	$0.0086 \pm 0.0000$	0.9927	$63.66 \pm 1.65\%$
53	$0.0144 \pm 0.0002$	0.9968	$82.88 \pm 0.85\%$
80	$0.0129 \pm 0.0011$	0.9954	$79.19 \pm 2.72\%$
106	$0.0126 \pm 0.0012$	0.9987	$78.02 \pm 2.01\%$

degradation increased with increasing tube diameter from 26 nm to 53 nm, while further increased tube diameters from 53 nm to 106 nm impose no significant effect. Increasing nanotube diameter would benefit light transmittance inside the nanotubes, resulting in a positive impact on the photoactivity of TNAs, according to a previous study [38]. Therefore, it is likely that certain nanotube diameter is needed to obtain good photoactivity of TNAs. In addition, the difference in specific surface areas of TNAs with varied diameter may also play a role. The change in specific surface area would not only influence the primary MTP degradation route, which involves reactive species in the liquid phase, by affecting diffusion of reactive species from TNAs surface to the liquid phase, but also affect the secondary MTP degradation route taking place on the TNAs surface via reaction with  $\text{h}^+$  and surface adsorbed hydroxyl radicals. The phenomenon observed in the present study was a result of the synergistic effect of the abovementioned two facts. To fully understand such synergistic effect, more advanced analysis are required, e.g. Electron Paramagnetic Resonance studies to provide more details on the diffusion behaviour of photo-generated reactive species from catalyst surface to the liquid phase.

**3.2.1.2.  $\text{TiO}_2$  nanotube arrays crystallographic phase.** In addition to tube diameter, crystallographic phase also exerts impact on photoactivity of TNAs [39]. Considering the satisfactory performance of TNAs with diameter  $\geq 53$  nm, the TNAs prepared under 20 V which have average diameter of 80 nm was chosen for further investigations. Performance of TNAs prepared under 20 V anodization potential with different crystallographic compositions was studied. The results (Fig. 7 and Table 4) show that crystallographic phase imposes significant impact on the photocatalytic degradation of MTP. Only a small portion ( $25.67 \pm 4.37\%$ ) of MTP was degraded over the as-prepared TNAs. This can be attributed to the fact that the as-prepared TNAs are majorly in amorphous phase (although very small amount of anatase is present), which has very low photoresponse. This is in line with literature reporting that amorphous structured  $\text{TiO}_2$  has very poor photocatalytic efficacy [40]. As aforementioned, by annealing the TNAs at 300 °C and 450 °C, the  $\text{TiO}_2$  NTs were converted to anatase form (Fig. 5). Therefore, identical kinetics values and total removal of MTP were obtained, when the TNAs annealed at 300 °C and 450 °C

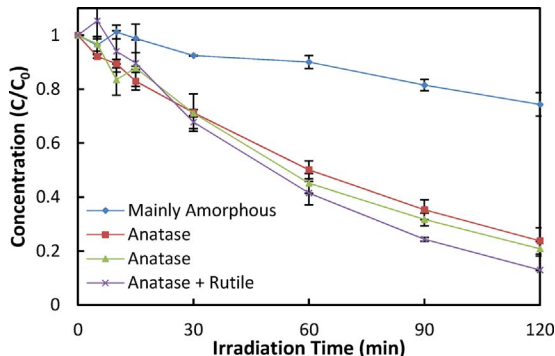


Fig. 7. Effect of  $\text{TiO}_2$  nanotube arrays crystalline phase composition on the photocatalytic MTP degradation.

**Table 4**

Effect of  $\text{TiO}_2$  nanotube arrays crystalline phase compositions on the kinetics of photocatalytic degradation of metoprolol.

Annealing temperature	crystalline phase	$k_{\text{app}}$ ( $\text{min}^{-1}$ )	$R^2$	Total removal
As-prepared	Mainly amorphous	$0.0023 \pm 0.0003$	0.9512	$25.67 \pm 4.37\%$
300 °C	Anatase	$0.0118 \pm 0.0015$	0.9989	$76.26 \pm 4.90\%$
450 °C	Anatase	$0.0129 \pm 0.0011$	0.9954	$79.19 \pm 2.72\%$
600 °C	Rutile	$0.0161 \pm 0.0005$	0.9819	$87.09 \pm 0.09\%$
	+ Anatase			

were applied. The highest pseudo-first order rate constant and total removal of MTP degradation were obtained when a mixture of anatase and rutile were present. The effect of crystalline phases on the photoactivity of  $\text{TiO}_2$  remains unclear, and debate still exists because the results of previous studies are not in line with each other. A study conducted by Macak et al. [40] compared the photocatalytic performance of amorphous, anatase phase, rutile phase, mixture of anatase and rutile phases, and the results show that the anatase phase has the highest photocatalytic performance. On the contrary, Liang and Li [51] reported that a mixture of anatase and rutile has highest photocatalytic performance on degradation of 2,3-dichlorophenol in aqueous solution. Anatase is well known for its better photoactivity. Rutile is known to have smaller band gap than anatase (3.2 eV for anatase and 3.0 eV for rutile) [47], and therefore better response to photons with longer wavelengths can be expected, which could promise an increase in photoactivity of the TNAs with its addition. On the other hand, usually faster recombination of  $e^-/\text{h}^+$  pairs happens in rutile [52] could exert negative impact on its photoactivity. Therefore, there should be an optimal rutile: anatase ratio, below or above which lower photocatalytic performance is obtained. In depth investigation on this aspect is of interest for optimization of TNAs. Taking into account that the highest pseudo-first order rate constant and total removal of MTP degradation were obtained when a mixture of anatase and rutile were present in TNAs, the TNAs prepared under 20 V anodization potential and annealed at 600 °C were used in the following sections.

### 3.2.2. Effect of initial concentration of metoprolol

MTP is reported to be present in various water bodies at very low concentration, at ng/L to  $\mu\text{g}/\text{L}$  level [12]. Considering this fact, to evaluate the applicability of the photocatalytic degradation of MTP using TNAs, it is of importance to examine how would the initial concentration of MTP affect the efficacy of the UV-LED/TNAs system. Photocatalytic experiments were performed with varied initial MTP concentrations, ranging from 0.1 mg/L to 1.5 mg/L, to examine this aspect. The efficacy was evaluated in terms of both pseudo-first order kinetic values and total removal of MTP after 120 min treatment. Unsurprisingly, the results (Fig. 8 and Table 5) show that both the degradation rate constant and total removal of MTP were not negatively affected by decreasing initial MTP concentration from 1.0 mg/L, and the MTP degradations followed pseudo-first order kinetics model when initial MTP concentration was in the range of 0.1–1.0 mg/L. On the other hand, decreased apparent rate constant and total removal of MTP were observed when initial MTP concentration was increased to 1.5 mg/L. This finding can be attributed to the following facts: (1) the availability of reactive species was constant under the same applied irradiation conditions and catalyst loading [53]; (2) when initial MTP concentration was 1.0 mg/L, the amount of reactive species was already at excess level, resulting in pseudo-first order degradation of MTP. When lower initial MTP concentration was applied, the reactive species to target pollutant ratio was further increased, therefore at lower initial MTP concentration the MTP degradation still followed the same pseudo-first order kinetics model. Consequently, lower initial MTP concentration imposed no negative impact on MTP degradation. The

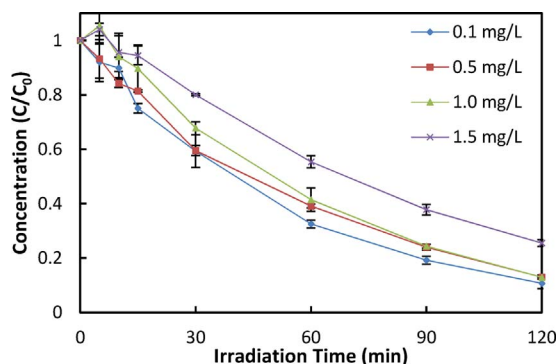


Fig. 8. Effect of initial concentration of metoprolol on the photocatalytic MTP degradation.

Table 5

Effect of initial concentration of metoprolol on the kinetics of photocatalytic metoprolol degradation.

Initial MTP concentration (mg/L)	$k_{app}$ ( $\text{min}^{-1}$ )	$R^2$	Total removal
0.1	$0.0185 \pm 0.0014$	0.9984	$89.27 \pm 2.04\%$
0.5	$0.0165 \pm 0.0004$	0.9968	$87.03 \pm 0.82\%$
1.0	$0.0161 \pm 0.0005$	0.9819	$87.09 \pm 0.09\%$
1.5	$0.0108 \pm 0.0005$	0.9780	$74.50 \pm 1.30\%$

analysis presented here is an indication that application of the UV-LED/TNAs photocatalytic degradation system in real-life may not be negatively affected by much more diluted MTP concentration, and it could assist further comprehensive studies assessing the performance of the UV-LED/TNAs system in real life implications.

### 3.2.3. Effect of pH

The effect of pH was examined in the range of 3–11 to study the applicability of the TNAs based photocatalytic pharmaceutical degradation processes, in terms of both degradation kinetics and total removal after 120 min treatment. The results (Table 6 and Fig. 9) reveal that the photocatalytic performance of TNAs on MTP degradation remains highly effective in a wide pH range, from 3 to 11. As demonstrated in Table 6 and Fig. 9, the UV-LED/TNAs system can be applied in a wide pH range: (1) even acute acidic conditions ( $pH_0 = 3$ ) imposes no adverse impact on the photocatalytic degradation of MTP; (2) a moderate decrease in MTP degradation was observed under acute basic conditions ( $pH_0 = 11$ ), but the overall performance was still comparable to that under neutral and acidic conditions. Plausible explanation of the decrease of photocatalytic MTP degradation over TNAs lies in the electrostatic repulsive effect between deprotonated MTP and TNAs surface. MTP has a  $pK_a$  value of 9.68 [54], making it deprotonated into negatively charged anion form. Meanwhile, under acute basic conditions ( $pH_0 = 11$ ) the TNAs surface was also negatively charged, according to literature [55]. Consequently, the electrostatic effect would make TNAs surface repulsive to the deprotonated MTP, which would pose a negative effect on the degradation of MTP. As addressed in the mechanistic section, although major MTP degradation occurred in the bulk liquid phase, secondary MTP degradation routes occurred on the surface TNAs (TNAs – liquid interface), involving either direct

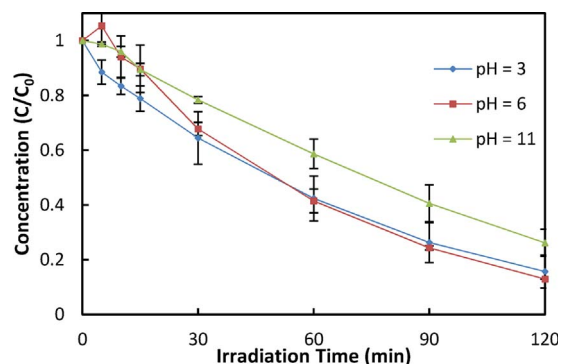


Fig. 9. Effect of initial pH on the photocatalytic MTP degradation.

oxidation by photo generated holes or hydroxyl radicals adsorbed on TNAs surface. The high pH induced repulsive effect of the TNAs surface towards deprotonated MTP molecules resulted in inhibition of the secondary MTP degradation route. The same effect of alkaline pH has been reported in a study conducted by Habibi et al. [21], where the effect of pH on slurry  $\text{TiO}_2$  photocatalytic degradation of Reactive Yellow 2 was examined and increasing pH was reported to cause decreased degradation efficiency of the dye.

### 3.2.4. Effect of inorganic ions

Regarding real life application of heterogeneous photocatalytic systems, presence of various inorganic ions should be taken into account, because many of them have been reported to pose detrimental effect even at low concentration levels [21,55,56]. Therefore, experiments were carried out to examine the effect of presence of some common inorganic ions, i.e. bicarbonate ions, phosphate ions. To best represent the real implication, HCl was used to adjust the reaction solutions with phosphate or bicarbonate addition to circum-neutral (6–7).

The obtained results (Fig. 10 and Table 7) show that the presence of both inorganic ions exerts no detrimental impact on the UV/TNAs photocatalytic degradation of MTP. Both the pseudo-first order rate constant and the total removal of MTP degradation were not negatively influenced by the presence of phosphate ions or bicarbonate ions at various concentration levels. Moreover, slight increase in the MTP degradation was obtained with the presence of phosphate ions or 50 mg/L bicarbonate ions. The obtained results herein exhibit great advantage of TNAs over conventional  $\text{TiO}_2$  slurry systems. Significant detrimental effect of bicarbonate and phosphate ions on the performance of conventional  $\text{TiO}_2$  slurry systems has been well documented in literature and examples are abundant [21,55,57,58]. In a study conducted by Rioja et al. [57] investigated the effect of water matrix on the photodegradation of clofibric acid, and found that even the presence of 50 mg/L  $\text{NaHCO}_3$  or  $\text{NaCO}_3$  caused significant decrease in the clofibric acid degradation. Another study conducted by Rincon et al. [58] investigated the effect of inorganic on photocatalytic inactivation of *E. Coli*, and reported that addition of bicarbonate and phosphate ions resulted in a meaningful decrease in photocatalytic *E. Coli* inactivation.

Although there is a generally known detrimental effect of carbonate species ( $\text{HCO}_3^-$  or  $\text{CO}_3^{2-}$ ) and phosphate species on AOPs, mainly due to scavenging of hydroxyl radicals, the possible positive impact should also be taken into account. For the carbonate species, by reacting with hydroxyl radicals, carbonate radicals are generated [59,60]. The carbonate radical has relatively high oxidizing potential ( $E_0 = 1.78 \text{ V}$  at pH 7) and tend to attack compounds with electron-rich moieties [59]. Besides, carbonate species can also act as conduction band electrons quencher [61], which decreases the recombination of  $e^-/\text{h}^+$  pairs and can in turn impose a positive impact on the photocatalytic degradation of MTP. To confirm the electron quenching capability of bicarbonate species, an additional experiment was conducted by irradiating a 200 mg/L bicarbonate aqueous solution with UV light in the presence of

Table 6

Effect of initial pH on the kinetics of photocatalytic metoprolol degradation.

Initial pH	$k_{app}$ ( $\text{min}^{-1}$ )	$R^2$	Total removal
3	$0.0151 \pm 0.0033$	0.9975	$84.29 \pm 6.00\%$
6	$0.0161 \pm 0.0005$	0.9819	$87.09 \pm 0.09\%$
11	$0.0104 \pm 0.0016$	0.9824	$73.83 \pm 4.95\%$

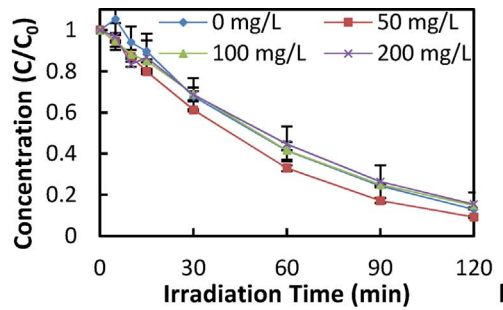
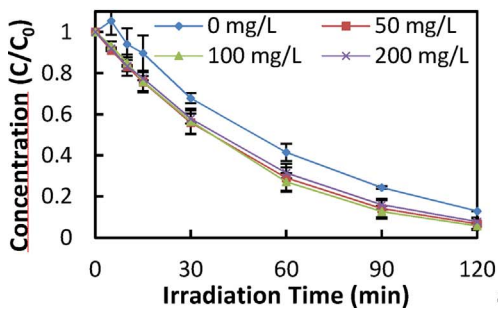


**Fig. 10.** Effect of inorganic ions on the photocatalytic MTP degradation: (a) phosphate ions (b) bicarbonate ions.

**Table 7**  
Effect of inorganic ions on the kinetics of photocatalytic metoprolol degradation.

Background water constituents	Concentration (mg/L)	$k_{app}$ (min <sup>-1</sup> )	R <sup>2</sup>	Total removal
No addition	0	0.0161 ± 0.0005	0.9819	87.09 ± 0.09%
Bicarbonate	50	0.0194 ± 0.006	0.9956	90.78 ± 0.51%
	100	0.0154 ± 0.004	0.9941	85.19 ± 0.82%
	200	0.0149 ± 0.0033	0.9913	84.57 ± 5.72%
	Phosphate	50	0.0219 ± 0.0040	0.9970
Phosphate	100	0.0231 ± 0.0024	0.9947	94.28 ± 1.47%
	200	0.0206 ± 0.0016	0.9965	92.19 ± 1.54%

TNA. The obtained results (Table SI 2) show that after 120 min irradiation, the total organic carbon of the solution increased from 0 mg/L to nearly 5 mg/L, which soundly support the hypothesis that the bicarbonate ions in the UV/TNAs system are able to rigorously quench conduction band electrons. To this end, the detrimental effect of bicarbonate induced by scavenging of hydroxyl radicals would be compensated by the formation of carbonate radicals and following carbonate radical mediated MTP degradation, as well as the quenching of conduction band electrons by bicarbonate ions. Therefore, the presence of bicarbonate in this study had no detrimental effect. For the presence of phosphate, the effect is also two-sided. On the one hand, it can adsorb on to the catalyst surface to decrease the adsorption of target pollutants and therefore hinder the degradation of target pollutants on the catalyst surface. However, previous studies have also pointed out that the adsorption of phosphate ions on the catalyst surface would lead to enhanced photocatalytic degradation of target pollutants by promoting the separation of e<sup>-</sup>/h<sup>+</sup> pairs via introducing electrostatic field on the catalyst surface [62]. Considering the fact that major MTP degradation takes place in the bulk liquid phase (as described in details in section 3.4), the adverse effect of phosphate can be neglected. Therefore, a slight increase in MTP degradation was obtained with presence of phosphate ions.

### 3.2.5. Effect of NOMs

Natural organic matters (NOMs) are present in broad range of water bodies and are known to be able to interfere with AOPs [63]. Given this context, to evaluate the applicability of TNAs for photocatalytic degradation of MTP, it is of interest to study the effect of NOMs and document the bearable NOMs concentrations range. Experiments were carried out in the presence of various NOMs concentrations from 5 mg/L to 15 mg/L (corresponding to TOC concentrations from 2 mg/L to 6 mg/L).

The obtained results (Fig. 11 and Table 8) indicate that the presence of NOMs at concentration levels ≤ 5 mg/L has no noteworthy detrimental effect. Both the pseudo-first-order rate constant and total removal of MTP remained at the same level, when 5 mg/L NOMs was added. With increased concentration levels, the NOMs started to exhibit a detrimental effect on the photocatalytic MTP degradation. The degradation rate constant decreased drastically from 0.0147 ± 0.0015 min<sup>-1</sup> to 0.0053 ± 0.0009 min<sup>-1</sup> when NOMs

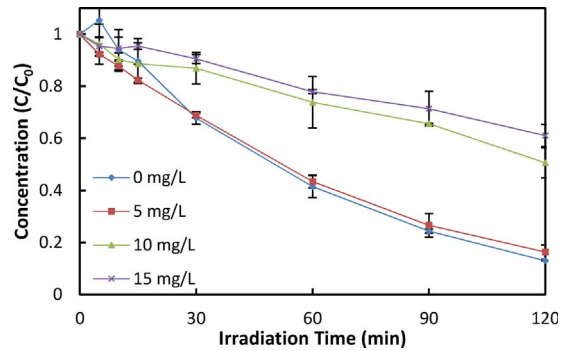


**Fig. 11.** Effect of NOMs on the photocatalytic MTP degradation.

**Table 8**  
Effect of NOMs on the kinetics of photocatalytic metoprolol degradation.

NOMs concentration (mg/L)	$k_{app}$ (min <sup>-1</sup> )	R <sup>2</sup>	Total removal
0	0.0161 ± 0.0005	0.9819	87.09 ± 0.09%
5	0.0147 ± 0.0015	0.9967	83.72 ± 2.78%
10	0.0053 ± 0.0009	0.9730	49.42 ± 5.76%
15	0.0040 ± 0.0007	0.9889	38.93 ± 4.20%

concentration increased from 5 mg/L to 10 mg/L, and the total removal of MTP decreased from 83.72 ± 2.78% to 49.42 ± 5.76%. Further decrease in MTP degradation was observed by increasing NOMs concentration to 15 mg/L: the degradation rate constant decreased to 0.0040 ± 0.0007 min<sup>-1</sup> and the total removal of MTP decreased to 38.93 ± 4.20%.

This observed phenomenon can be attributed to the characteristics of NOMs. The NOMs have light absorption in UV and near UV range (See Figure SI 3 in supplementary materials). Moreover, NOMs can also act as reactive species quencher, which in turn decrease the availability of reactive species for MTP degradation. Therefore, they impose a detrimental effect on photocatalytic MTP degradation over TNAs.

Although it is also documented that NOMs can act as photosensitizer which may mitigate its detrimental effect on target pollutant degradation, the experimental data (Figure SI 4) suggest that NOMs do not act as photosensitizer in the UV-LED/TNAs system under the applied conditions.

### 3.2.6. Efficacy of the TiO<sub>2</sub> nanotube arrays on photocatalytic metoprolol degradation in tap water

To further evaluate the applicability of the TNAs, an experiment was carried out with tap water to examine the efficacy of photocatalytic MTP degradation by using TNAs as photocatalyst. The pseudo-first order kinetic constant and total removal of MTP degradation demonstrated in Fig. 12 and Table 9. The results show that the degradation rate constants experienced a decrease from 0.0161 ± 0.0005 min<sup>-1</sup> in Milli-Q water to the value of 0.0076 ± 0.0001 min<sup>-1</sup> in tap water. The total removal of MTP after 120 min of photocatalytic treatment over TNAs decreased from 87.09 ± 0.09% in Milli-Q water to

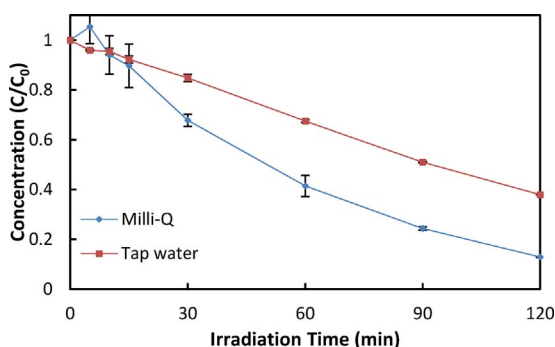


Fig. 12. Effect of water matrices on the photocatalytic MTP degradation.

Table 9

Comparison of the kinetics of photocatalytic metoprolol degradation in tap water and Milli-Q water.

Water matrix	$k_{app}$ ( $\text{min}^{-1}$ )	$R^2$	Total removal
Milli-Q	$0.0161 \pm 0.0005$	0.9819	$87.09 \pm 0.09\%$
Tap water	$0.0076 \pm 0.0001$	0.9849	$62.05 \pm 0.08\%$

$62.05 \pm 0.08\%$  in tap water. The characteristics of the tap water were shown in Table SI 1. Although bicarbonate and phosphate ions exhibit no detrimental effect on the photocatalytic degradation of MTP over TNAs as shown in previous section, the degradation of MTP would still be interfered by the presence of other organic compounds in tap water. Those organic compounds would compete with the target pollutant for oxidizing species, screen UV irradiation, and may also adsorb onto the photocatalyst surface [64]. On the contrary to TNAs based, conventional  $\text{TiO}_2$  slurry system was much more vulnerable to the matrix. In a previous study conducted by Rioja et al. [57], it is reported that the target pollutant degradation rate constant decreased drastically from  $0.3468 \text{ min}^{-1}$  in pure water to  $0.0033 \text{ min}^{-1}$  in tap water.

### 3.3. Contribution of different photo-induced reactive species

Previous studies on  $\text{TiO}_2$  based photocatalytic systems have pointed out that hydroxyl radicals are vital reactive species in degradation of target-pollutants [23]. However, some researchers clearly pointed out that other species, including electrons, holes, superoxide anion radicals, singlet oxygen, can also contribute to degradation of target-pollutants depending on the characteristics of specific catalyst [47]. Viewing this fact, in order to evaluate the mechanistic aspect, experiments with addition of specific scavengers were carried out. The results demonstrate that the degradation of MTP was greatly hindered: total removal after 120 min treatment was decreased to  $2.42 \pm 2.19\%$  and  $10.48 \pm 0.50\%$ , with addition formic acid and *tert*-butanol respectively.

Knowing the fact that formic acid can rigorously quench photo generated electron holes ( $\text{h}^+$ ) on the surface of TNAs once they were produced, addition of formic acid in the reaction hindered not only the degradation pathway mediated by electron holes but also degradation pathways with participation of hydroxyl radicals [47]. Due to extreme low affinity to  $\text{TiO}_2$  surfaces, the *tert*-butanol only scavenges hydroxyl radicals in bulk liquid phase. From the obtained results, the contribution of different degradation routes was obtained. As shown in Fig. 13, the primary photocatalytic degradation of MTP occurred via reaction with hydroxyl radicals in bulk liquid phase, which accounts for 88% of the MTP removal. In a recent study conducted by Arlos et al. [29], it is reported that highly mobility of hydroxyl radicals allows them diffuse from the surface to liquid phase and therefore interact with compounds in the liquid phase, and hence adsorption of target contaminants on catalyst surface is not necessarily a pre-requisite for efficient

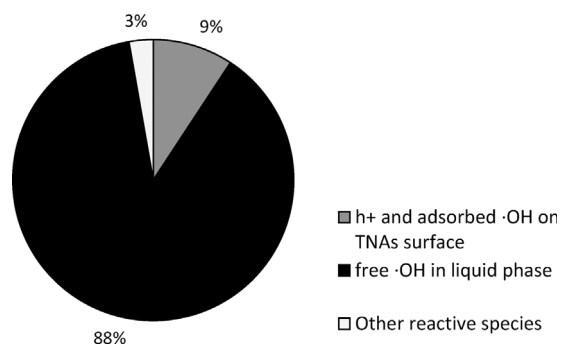


Fig. 13. Contribution of different reactive species on the MTP degradation.

photocatalytic degradation of target-pollutants. This is in accordance with the present study: only very small portion of MTP degradation occurred on the surface of TNAs (TNAs – liquid interface), degraded by either direct oxidation by photo generated holes or hydroxyl radicals adsorbed on TNAs surface. Additionally, it should be noticed that other reactive species, likely to be superoxide anion radicals according to literature [47], did also play a minor role in MTP degradation over TNAs, which accounts for around 3% of the MTP removal. This finding in this study is in agreement with previous studies on  $\text{TiO}_2$  photocatalytic MTP removal processes [47]. A schematic of the MTP degradation over TNAs was proposed as shown in Fig. 14.

This finding was further confirmed via by-products analysis by LC-MS/MS. The LC-MS/MS analysis show that the UV/TNAs photocatalytic degradation of MTP resulted in formation of 25 main degradation by-products (DP). The  $m/z$  ratios and corresponding retention times (RT) of detected DPs are summarized in Table SI 3, and the evolution of those DPs versus time was summarized in Figure SI 7. The obtained DPs are in agreement with previous studies using  $\text{TiO}_2$  for MTP removal [12,47,64], and tentative structures of those DPs have been proposed by a previous study [64]. By inhibiting the participation of holes and  $\cdot\text{OH}$ , most of the DPs were not formed, and only DP3 ( $m/z = 134$ , RT = 1.22 min), DP4 ( $m/z = 76$ , RT = 1.23 min), DP6 ( $m/z = 120$ , RT = 1.23 min), and DP23 ( $m/z = 284$ , RT = 5.45 min) were observed. By inhibiting the participation of  $\cdot\text{OH}$  in the bulk liquid phase, DP3, DP4, DP6, DP23, and DP24 ( $m/z = 282$ , RT = 5.66 min) were obtained.

### 3.4. Stability of $\text{TiO}_2$ nanotube arrays

Stability of the TNAs was evaluated under acidic ( $\text{pH}_0 = 3$ ), neutral ( $\text{pH}_0 = 6$ ), and alkaline conditions ( $\text{pH}_0 = 11$ ) in terms of their reuse performance over 6 cycles. For each cycle, the treatment time was 120 min. The TNAs were washed by Milli-Q water and dried in  $\text{N}_2$  stream at ambient temperature after each run, and were then reused in subsequent run. As demonstrated in Fig. 15, photocatalytic MTP degradation by TNAs was not negatively affected during the repeated treatment cycles under different operation conditions, revealing relatively good stability of the TNAs and its potential in real life implications.

## 4. Conclusions

The synthesis of self-organized  $\text{TiO}_2$  nanotube arrays (TNAs) and their application for photocatalytic degradation of a  $\beta$ -blocker metoprolol (MTP) was studied. Self-organized TNAs are found to be a powerful catalyst for photocatalytic removal of MTP from aqueous streams. Main conclusions can be drawn from our results are summarized herein:

- For fabrication of self-organized TNAs, anodization potential and annealing temperature are two key parameters which control the

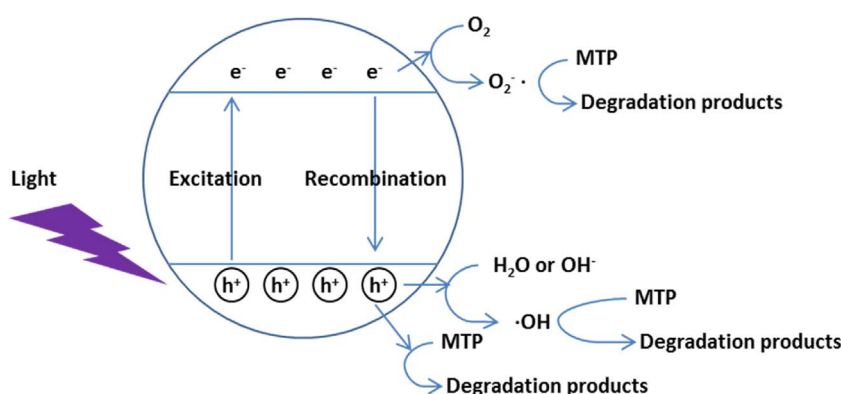


Fig. 14. Proposed schematic photocatalytic degradation mechanism of MTP over TNAs.

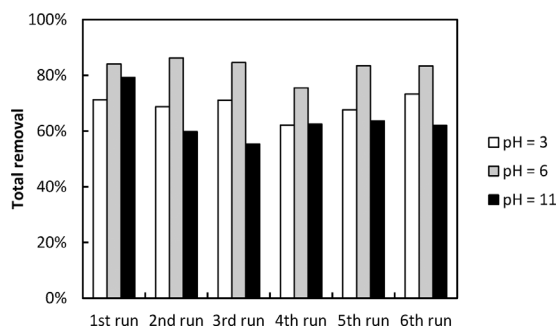


Fig. 15. Total removal of MTP after 120 min photocatalytic treatment over TNAs for repeated use at different pH conditions.  $[MTP]_0 = 1 \text{ mg/L}$ .

diameter and crystallographic composition of the anodic produced  $\text{TiO}_2$  nanotubes respectively.

- The surface morphology and crystallographic composition of the anodic produced  $\text{TiO}_2$  nanotubes impose impact on performance of the TNAs in photocatalytic MTP degradation, respectively. For TNAs with given average nanotube diameters, photocatalytic MTP degradation was favoured when a mixture of anatase and rutile was present in the TNAs structure; for TNAs with certain crystallographic composition, rapid MTP degradation was obtained when the nanotubes diameter reached 53 nm
- The UV-LED/TNAs system can be applied in a wide pH range, and lower initial MTP concentration imposed no negative impact on MTP degradation. The analysis presented here is an indication that application of the UV-LED/TNAs photocatalytic degradation system in real-life may not be negatively affected by much more diluted MTP concentration, and it could assist further comprehensive studies assessing the performance of the UV-LED/TNAs system in real life implications.
- Regarding real life application, the presence of even high level bicarbonate ions and phosphate ions has no detrimental effect, while NOMs concentration higher than 5 mg/L does negatively affect the photocatalytic degradation of MTP. Operation in real tap water samples leaded to a slight decrease in the process efficiency, but the performance was still reasonable.
- The obtained results demonstrate that primary degradation process occurred in liquid phase with participation of hydroxyl radicals in the liquid phase ( $\cdot\text{OH}_{\text{liquid}}$ ), while smaller portion of MTP were degraded on the catalyst surface via reaction with  $\text{h}^+$  and hydroxyl radicals adsorbed on the catalyst surface ( $\cdot\text{OH}_{\text{surface}}$ ). Other reactive species, e.g. photo generated electrons and superoxide radical anions, did also play a minor role in MTP degradation. The mechanistic aspect was further confirmed by identification of degradation products by LC-MS/MS.
- The TNAs exhibit good stability during repeated treatment cycles, which is an indication of its potential in real life implications. To

fully understand its applicability in real life implications, further research efforts are required, for instance the performance of TNAs during long time operation in the presence of various inorganics and other pollutants, and also the synergistic effect of co-existence of inorganics and other organics on the performance of the catalyst and cost of operation of the system should be evaluated systematically.

#### Acknowledgements

This work was performed in the cooperation framework of Wetsus, European Centre of Excellence for Sustainable Water Technology ([www.wetsus.eu](http://www.wetsus.eu)). Wetsus is co-funded by the Dutch Ministry of Economic Affairs and Ministry of Infrastructure and Environment, the Province of Fryslân, and the Northern Netherlands Provinces. The authors would like to thank the participants of the research theme “Advanced water treatment” for the fruitful discussions and their financial support. The authors gratefully thank Ton van der Zande and Mieke Kersaen-Han for the realization of the instrumental analysis, and Dr. Sofia Semitsoglou-Tsiapou and Dr. Maarten Biesheuvel for the fruitful discussions.

#### Appendix A. Supplementary data

Supplementary data associated with this article can be found, in the online version, at <http://dx.doi.org/10.1016/j.apcatb.2017.08.040>.

#### References

- P. Verlicchi, M. Al Aukidy, E. Zambello, Occurrence of pharmaceutical compounds in urban wastewater: removal, mass load and environmental risk after a secondary treatment – A review, *Sci. Total Environ.* 429 (2012) 123–155.
- A. Nikolaou, S. Meric, D. Fatta, Occurrence patterns of pharmaceuticals in water and wastewater environments, *Anal. Bioanal. Chem.* 387 (2007) 1225–1234.
- M. Klavarioti, D. Mantzavinos, D. Kassinos, Removal of residual pharmaceuticals from aqueous systems by advanced oxidation processes, *Environ. Int.* 35 (2009) 402–417.
- M. Sánchez-Polo, J. Rivera-Utrilla, G. Prados-Joya, R. Ocampo-Pérez, Metronidazole photodegradation in aqueous solution by using photosensitizers and hydrogen peroxide, *J. Chem. Technol. Biot.* 87 (2012) 1202–1208.
- C. Martínez, M. Canle L, M.I. Fernández, J.A. Santaballa, J. Faria, Aqueous degradation of diclofenac by heterogeneous photocatalysis using nanostructured materials, *Appl. Catal. B: Environ.* 107 (2011) 110–118.
- C. Tixier, H.P. Singer, S.R. Oellers, S.R. Müller, Occurrence and fate of carbamazepine, clofibric acid, diclofenac, ibuprofen, ketoprofen, and naproxen in surface waters, *Environ. Sci. Technol.* 37 (2003) 1061–1068.
- R. Andreozzi, M. Raffaele, P. Nicklas, Pharmaceuticals in STP effluents and their solar photodegradation in aquatic environment, *Chemosphere* 50 (2003) 1319–1330.
- T.E. Doll, F.H. Frimmel, Fate of pharmaceuticals-photodegradation by simulated solar UV-light, *Chemosphere* 52 (2003) 1757–1769.
- T.A. Ternes, M. Meisenheimer, D. McDowell, F. Sacher, H.-J. Brauch, B. Haist-Gulde, G. Preuss, U. Wilme, N. Zulei-Seibert, Removal of pharmaceuticals during drinking water treatment, *Environ. Sci. Technol.* 36 (2002) 3855–3863.
- E. Díez-Mato, F.C. Cortezón-Tamarit, S. Bogialli, D. García-Fresnadillo, M.D. Marazuela, Phototransformation of model micropollutants in water samples by photocatalytic singlet oxygen production in heterogeneous medium, *Appl. Catal. B: Environ.* 160–161 (2014) 445–455.

- [11] L.A. Ioannou, E. Hapeshi, M.I. Vasquez, D. Mantzavinos, D. Fatta-Kassinos, Solar/TiO<sub>2</sub> photocatalytic decomposition of  $\beta$ -blockers atenolol and propranolol in water and wastewater, *Sol. Energy* 85 (2011) 1915–1926.
- [12] R.P. Cavalcante, R.F. Dantas, B. Bayarri, O. González, J. Giménez, S. Esplugas, A. Machulek Junior, Synthesis and characterization of B-doped TiO<sub>2</sub> and their performance for the degradation of metoprolol, *Catal. Today* 252 (2015) 27–34.
- [13] M.D. Hernando, M. Mezcua, A.R. Fernández-Alba, D. Barceló, Environmental risk assessment of pharmaceutical residues in wastewater effluents, surface waters and sediments, *Talanta* 69 (2006) 334–342.
- [14] D.B. Huggett, B.W. Brooks, B. Peterson, C.M. Foran, D. Schlenk, Toxicity of select beta adrenergic receptor-Blocking pharmaceuticals (B-Blockers) on aquatic organisms, *Arch. Environ. Contam. Toxicol.* 43 (2002) 229–235.
- [15] D. Vogna, R. Marotta, A. Napolitano, R. Andreozzi, M. d'Ischia, Advanced oxidation of the pharmaceutical drug diclofenac with UV/H<sub>2</sub>O<sub>2</sub> and ozone, *Water Res.* 38 (2004) 414–422.
- [16] J.M. Poyatos, M.M. Muñio, M.C. Almecija, J.C. Torres, E. Hontoria, F. Osorio, Advanced Oxidation Processes for Wastewater Treatment: State of the Art, Water, Air and Soil Pollution 205 (2009), pp. 187–204.
- [17] J.J. Pignatello, E. Oliveros, A. MacKay, Advanced oxidation processes for organic contaminant destruction based on the fenton reaction and related chemistry, *Critical Rev. Environ. Sci. Technol.* 36 (2006) 1–84.
- [18] Z. Liu, X. Zhang, S. Nishimoto, T. Murakami, A. Fujishima, Efficient photocatalytic degradation of gaseous acetaldehyde by highly ordered TiO<sub>2</sub> nanotube arrays, *Environ. Sci. Technol.* 42 (2008) 8547–8551.
- [19] J. Kuipers, Distributed light sources for photocatalytic water treatment, University Wageningen, Wageningen, 2014.
- [20] C.S. Chiou, J.L. Shie, C.Y. Chang, C.C. Liu, C.T. Chang, Degradation of di-n-butyl phthalate using photoreactor packed with TiO<sub>2</sub> immobilized on glass beads, *J. Hazard. Mater.* 137 (2006) 1123–1129.
- [21] M.H. Habibi, A. Hassanzadeh, S. Mahdavi, The effect of operational parameters on the photocatalytic degradation of three textile azo dyes in aqueous TiO<sub>2</sub> suspensions, *J. Photochem. Photobiol. A: Chem.* 172 (2005) 89–96.
- [22] A. Achilleos, E. Hapeshi, N.P. Xekoukoulakis, D. Mantzavinos, D. Fatta-Kassinos, Factors affecting diclofenac decomposition in water by UV-A/TiO<sub>2</sub> photocatalysis, *Chem. Eng. J.* 161 (2010) 53–59.
- [23] M. Canle L, J.A. Santaballa, E. Vulliet, On the mechanism of TiO<sub>2</sub>-photocatalyzed degradation of aniline derivatives, *J. Photochem. Photobiol. A: Chem.* 175 (2005) 192–200.
- [24] J. Chen, D.F. Ollis, W.H. Rulkens, H. Bruning, Photocatalyzed oxidation of alcohols and organochlorides in the presence of native TiO<sub>2</sub> and metallized TiO<sub>2</sub> suspensions. Part (I): Photocatalytic activity and pH influence, *Water Res.* 33 (1999) 661–668.
- [25] M. Dijkstra, A. Michorius, H. Buwalda, H. Panneman, J. Winkelmann, A. Beenackers, Comparison of the efficiency of immobilized and suspended systems in photocatalytic degradation, *Catal. Today* 66 (2001) 487–494.
- [26] M. Dijkstra, H. Panneman, J. Winkelmann, J. Kelly, A. Beenackers, Modeling the photocatalytic degradation of formic acid in a reactor with immobilized catalyst, *Chem. Eng. Sci.* 57 (2002) 4895–4907.
- [27] Y. He, N.B. Sutton, H.H.H. Rijnaarts, A.A.M. Langenhoff, Degradation of pharmaceuticals in wastewater using immobilized TiO<sub>2</sub> photocatalysis under simulated solar irradiation, *Appl. Catal. B: Environ.* 182 (2016) 132–141.
- [28] G. Mascolo, R. Comparelli, M.L. Curri, G. Lovecchio, A. Lopez, A. Agostiano, Photocatalytic degradation of methyl red by TiO<sub>2</sub>: Comparison of the efficiency of immobilized nanoparticles versus conventional suspended catalyst, *J. Hazard. Mater.* 142 (2007) 130–137.
- [29] M.J. Arlos, M.M. Hatat-Fraile, R. Liang, L.M. Bragg, N.Y. Zhou, S.A. Andrews, M.R. Servos, Photocatalytic decomposition of organic micropollutants using immobilized TiO<sub>2</sub> having different isoelectric points, *Water Res.* 101 (2016) 351–361.
- [30] J.C. Cardoso, T.M. Lizier, M.V.B. Zanoni, Highly ordered TiO<sub>2</sub> nanotube arrays and photoelectrocatalytic oxidation of aromatic amine, *Appl. Catal. B: Environ.* 99 (2010) 96–102.
- [31] Y. Zhao, N. Hoivik, K. Wang, Recent advance on engineering titanium dioxide nanotubes for photochemical and photoelectrochemical water splitting, *Nano Energy* 30 (2016) 728–744.
- [32] C.B. Marien, T. Cottineau, D. Robert, P. Drogui, TiO<sub>2</sub> Nanotube arrays: influence of tube length on the photocatalytic degradation of Paraquat, *Appl. Catal. B: Environ.* 194 (2016) 1–6.
- [33] X. Nie, J. Chen, G. Li, H. Shi, H. Zhao, P.K. Wong, T. An, Synthesis and characterization of TiO<sub>2</sub> nanotube photoanode and its application in photoelectrocatalytic degradation of model environmental pharmaceuticals, *J. Chem. Technol. Biotechnol.* 88 (2013) 1488–1497.
- [34] V. Zwilling, M. Aucouturier, E. Darque-Ceretti, Anodic oxidation of titanium and TA6 V alloy in chromic media. An electrochemical approach, *Electrochim. Acta* 45 (1999) 921–929.
- [35] V. Zwilling, E. Darque-Ceretti, A. Boutry-Forveille, D. David, M.-Y. Perrin, M. Aucouturier, Structure and physicochemistry of anodic oxide films on titanium and TA6 V alloy, *Surf. Interface Anal.* 27 (1999) 629–637.
- [36] J. Macak, H. Tsuchiya, A. Ghicov, K. Yasuda, R. Hahn, S. Bauer, P. Schmuki, TiO<sub>2</sub> nanotubes: self-organized electrochemical formation, properties and applications, *Curr. Opin. Solid State Mater. Sci.* 11 (2007) 3–18.
- [37] P. Roy, S. Berger, P. Schmuki, TiO<sub>2</sub> nanotubes: synthesis and applications, *Angew. Chem. Int. Ed.* 50 (2011) 2904–2939.
- [38] H.-F. Zhuang, C.-J. Lin, Y.-K. Lai, L. Sun, J. Li, Some critical structure factors of titanium oxide nanotube array in its photocatalytic activity, *Environ. Sci. Technol.* 41 (2007) 4735–4740.
- [39] Y.R. Smith, A. Kar, V. Subramanian, Investigation of physicochemical parameters that influence photocatalytic degradation of methyl orange over TiO<sub>2</sub> nanotubes, *Ind. Eng. Chem. Res.* 48 (2009) 10268–10276.
- [40] J.M. Macak, M. Zlamal, J. Krysa, P. Schmuki, Self-organized TiO<sub>2</sub> nanotube layers as highly efficient photocatalysts, *small* 3 (2007) 300–304.
- [41] T.S. Natarajan, K. Natarajan, H.C. Bajaj, R.J. Tayade, Energy efficient UV-LED source and TiO<sub>2</sub> nanotube array-based reactor for photocatalytic application, *Ind. Eng. Chem. Res.* 50 (2011) 7753–7762.
- [42] W.-K. Jo, R.J. Tayade, New generation energy-Efficient light source for photocatalysis, *LEDs Environ. Appl. Indus. Eng. Chem. Res.* 53 (2014) 2073–2084.
- [43] T.S. Natarajan, M. Thomas, K. Natarajan, H.C. Bajaj, R.J. Tayade, Study on UV-LED/TiO<sub>2</sub> process for degradation of Rhodamine B dye, *Chem. Eng. J.* 169 (2011) 126–134.
- [44] H.-W. Chen, Y. Ku, A. Irawan, Photodecomposition of o-cresol by UV-LED/TiO<sub>2</sub> process with controlled periodic illumination, *Chemosphere* 69 (2007) 184–190.
- [45] K. Natarajan, T.S. Natarajan, H.C. Bajaj, R.J. Tayade, Photocatalytic reactor based on UV-LED/TiO<sub>2</sub> coated quartz tube for degradation of dyes, *Chem. Eng. J.* 178 (2011) 40–49.
- [46] G.G. Bessegato, J.C. Cardoso, M.V.B. Zanoni, Enhanced photoelectrocatalytic degradation of an acid dye with boron-doped TiO<sub>2</sub> nanotube anodes, *Catal. Today* 240 (2015) 100–106.
- [47] R.P. Cavalcante, R.F. Dantas, B. Bayarri, O. González, J. Giménez, S. Esplugas, A. Machulek Junior, Photocatalytic mechanism of metoprolol oxidation by photocatalysts TiO<sub>2</sub> and TiO<sub>2</sub> doped with 5% B: Primary active species and intermediates, *Appl. Catal. B: Environ.* 194 (2016) 111–122.
- [48] Y. Ye, H. Bruning, D. Yntema, M. Mayer, H. Rijnaarts, Homogeneous photo-sensitized degradation of pharmaceuticals by using red light LED as light source and methylene blue as photosensitizer, *Chem. Eng. J.* 316 (2017) 872–881.
- [49] K. Yasuda, P. Schmuki, Control of morphology and composition of self-organized zirconium titanate nanotubes formed in (NH<sub>4</sub>)<sub>2</sub>SO<sub>4</sub>/NH<sub>4</sub>F electrolytes, *Electrochim. Acta* 52 (2007) 4053–4061.
- [50] J. Macak, H. Hildebrand, U. Marten-Jahns, P. Schmuki, Mechanistic aspects and growth of large diameter self-organized TiO<sub>2</sub> nanotubes, *J. Electroanal. Chem.* 621 (2008) 254–266.
- [51] H.-c. Liang, X.-z. Li, Effects of structure of anodic TiO<sub>2</sub> nanotube arrays on photocatalytic activity for the degradation of 2,3-dichlorophenol in aqueous solution, *J. Hazard. Mater.* 162 (2009) 1415–1422.
- [52] S. Sreekantan, R. Hazan, Z. Lockman, Photoactivity of anatase-rutile TiO<sub>2</sub> nanotubes formed by anodization method, *Thin Solid Films* 518 (2009) 16–21.
- [53] E. Regulska, D.M. Brus, P. Rodziewicz, S. Sawicka, J. Karpinska, Photocatalytic degradation of hazardous Food Yellow 13 in TiO<sub>2</sub> and ZnO aqueous and river water suspensions, *Catal. Today* 266 (2016) 72–81.
- [54] D.W. Newton, R.B. Kluza, pKa values of medicinal compounds in pharmacy practice, *Ann. Pharmacother.* 12 (1978) 546–554.
- [55] M.N. Chong, B. Jin, C.W.K. Chow, C. Saint, Recent developments in photocatalytic water treatment technology: a review, *Water Res.* 44 (2010) 2997–3027.
- [56] N. Daneshvar, S. Aber, M.S. Dorraji, A. Khataee, M. Rasoulifard, Photocatalytic degradation of the insecticide diazinon in the presence of prepared nanocrystalline ZnO powders under irradiation of UV-C light, *Sep. Purif. Technol.* 58 (2007) 91–98.
- [57] N. Rioja, S. Zorita, F.J. Peñas, Effect of water matrix on photocatalytic degradation and general kinetic modeling, *Appl. Catal. B: Environ.* 180 (2016) 330–335.
- [58] A.-G. Rincón, C. Pulgarín, Effect of pH, inorganic ions, organic matter and H<sub>2</sub>O<sub>2</sub> on *E. coli* K12 photocatalytic inactivation by TiO<sub>2</sub>: Implications in solar water disinfection, *Appl. Catal. B: Environ.* 51 (2004) 283–302.
- [59] W.W.-P. Lai, M.-H. Hsu, A.Y.-C. Lin, The role of bicarbonate anions in methotrexate degradation via UV/TiO<sub>2</sub>: Mechanisms, reactivity and increased toxicity, *Water Res.* 112 (2017) 157–166.
- [60] G.V. Buxton, C.L. Greenstock, W.P. Helman, A.B. Ross, Critical Review of rate constants for reactions of hydrated electrons, hydrogen atoms and hydroxyl radicals (-OH/-O- in aqueous Solution, *J. Phys. Chem. Ref. Data* 17 (1988) 513–886.
- [61] Y. Ku, W.-H. Lee, W.-Y. Wang, Photocatalytic reduction of carbonate in aqueous solution by UV/TiO<sub>2</sub> process, *J. Mol. Catal. A: Chem.* 212 (2004) 191–196.
- [62] D. Zhao, C. Chen, Y. Wang, H. Ji, W. Ma, L. Zang, J. Zhao, Surface modification of TiO<sub>2</sub> by phosphate: effect on photocatalytic activity and mechanism implication, *J. Phys. Chem. C* 112 (2008) 5993–6001.
- [63] J. Brame, M. Long, Q. Li, P. Alvarez, Trading oxidation power for efficiency: differential inhibition of photo-generated hydroxyl radicals versus singlet oxygen, *Water Res.* 60 (2014) 259–266.
- [64] R.P. Cavalcante, R.F. Dantas, H. Wender, B. Bayarri, O. González, J. Giménez, S. Esplugas, A. Machulek Jr., Photocatalytic treatment of metoprolol with B-doped TiO<sub>2</sub>: Effect of water matrix, toxicological evaluation and identification of intermediates, *Appl. Catal. B: Environ.* 176–177 (2015) 173–182.